Photo-induced generation of size controlled Au nanoparticles on pure siliceous ordered mesoporous silica for catalytic applications

Nghia Huu Le, Samar Hajjar-Garreau, Magali Bonne, Cristina Megias Sayago, Benoit Louis, Bénédicte Lebeau, Lavinia Balan

Photo-induced generation of size controlled Au nanoparticles on ordered mesoporous silica for catalytic applications

Nghia Huu Le[1,2], Samar Hajjar-Garreau[1,2], Magali Bonne[1,2]*, Cristina Megías-Sayago[3], Benoît Louis[3], Bénédicte Lebeau[1,2], Lavinia Balan[1,2]*

[1] Université de Haute Alsace (UHA), CNRS, IS2M UMR 7361, 68100 Mulhouse, France

[2] Université de Strasbourg, 67000 Strasbourg, France

[3] Université de Strasbourg, CNRS, ICPEES UMR 7515, ECPM, 67087 Strasbourg Cedex, France

* Corresponding author: E-mail address: magali.bonne@uha.fr, lavinia.balan@uha.fr

Abstract

A versatile *in situ* photochemical reduction approach was used to generate a composite of gold nanoparticles and SBA-15 silica support with regular mesopores. The mesoporous silica support was first synthesized and, after calcination, was suspended in a solution of gold bromide (EtOH or H_2O) containing a free radical generator activated by UV irradiation and used for the photochemical reduction of gold precursor. The influence of gold precursor concentration, light intensity and nature of the solvents on the formation and properties of gold nanoparticles (size, dispersion, stability) on the mesoporous SBA-15 support have been studied with the aim of

optimizing the dispersion of the gold nanoparticles in the mesoporous network and their chemical stability. The catalytic activity of the resulting AuNPs@SBA-15 nanocomposite was successfully evaluated for the oxidation of benzyl alcohol reaction in liquid-phase.

Keywords: Mesoporous silica, SBA-15, Gold nanoparticles, Photoreduction, Oxidation, Benzyl alcohol

1. Introduction

The combination of a solid support with noble metal nanoparticles leads to nanocomposites with specific properties [1]. Today, due to the diversity of synthetic methods and applications in various fields, gold-based nanocomposite materials are attracting a lot of attention.

In studies reported on the elaboration of gold-based nanocomposites, a particular interest was paid to the structural and textural properties of the support phases as well as to the formation and the properties of gold nanoparticles. Mesoporous gold-silica nanocomposites have been synthesized via sol-gel process and their optical properties were investigated for a promising application to detect the presence of trace amounts (10 ppm) of cyanide ion in aqueous solutions [2]. Gold / polyaniline composite materials have been prepared by a chemical reduction of chloroauric acid in methanol as solvent. Such composite materials, which contain gold nanoparticles stabilized by the polyaniline film matrix, exhibit controllable electric conduction properties [3]. A particular interest is the catalytic action of gold in the field of depollution (e.g. low temperature CO oxidation, NOx reduction, decomposition of ozone and volatile organic compounds (VOC), elimination of dioxins) [4–7] and, more recently, in the field of biomass valorisation (oxidation of lignocellulosic biomass derivatives such as glucose or 5-hydroxymethylfurfural to value-added compounds) [8,9]. In relation to the potential

transformation of biomass, the selective oxidation of alcohols to their corresponding aldehydes and ketones is of great importance in organic synthesis on both laboratory and industrial scales [10]. Derived from lignin fraction, benzyl alcohol conversion to benzaldehyde has attracted the scientific attention in the last decade [11–13]. The general reaction is presented in the Supplementary Information Section (Scheme A.1).

The catalytic properties of gold are related to the size of gold nanoparticles. In some cases, they must be narrower than 5 nm, which request the development of new synthetic methods [14,15]. Most of the methods used to generate gold nanoparticles are bottom-up methods, because the control of their state and shape is quite easy [16–27]. The different bottom-up methods, which can be distinguished from the reduction methods used for the generation of gold nanoparticles, are divided into different categories: the first one is based on chemical approaches (use of chemical reducing agents), the second one involves physical approaches (use of ultrasonic methods, electrochemistry, ionizing radiations) and another one is based on photo-assisted methods (UV irradiation, laser photolysis). The photochemical approach is based on the solvent (water or alcohol) decomposition by an ionizing radiation (electron beam), which leads to the formation of hydroxyl radicals and solvated electrons. These electrons, which are regarded as the most efficient reductive species, allow reducing a large number of metals ions [28–30].

$H_2O \rightarrow \bullet H, H_3O^+, e^-_{aq}, \bullet OH, H_2, H_2O_2$

$RCH_2OH \rightarrow \bullet H, H_3O^+, e^-_{aq}, RCH\bullet OH, H_2, H_2O$

The most widely used chemical approaches are based on the chemical reduction of gold ions in solution to form colloidal nanoparticles using sodium borohydride ($NaBH_4$) as a reducing agent [19,20]. Despite the popular utilization of $NaBH_4$, the reduction can also be carried out with trisodium citrate ($Na_3C_6H_5O_7$) [21] and a variety of other reducing agents such as oxalic acid,

hydrazine,…[16,22,23] These approaches involve the reduction of gold ions and the chemical / physical sorption of ligands at the surface of nanoparticles to prevent coagulation and precipitation. The reduction of gold ions could also take place in gas phase with dihydrogen as a reducing agent (pure or mixed with an inert gas) [24,25]. The disadvantage of chemical approaches is the presence of impurities in the reagents. Some approaches based on high temperature thermal reduction in air for a few hours have been also reported for the formation of gold nanoparticles [26,27]. However, these thermal strategies are much less used than those based on chemical reduction because of the propensity of nanoparticles to aggregate significantly at high temperature.

In the present work, an innovative photochemical approach, still rather infrequent, has been used for the reduction of gold precursors. Indeed, this photochemical method offers many advantages such as rapidity, mild conditions (reactions at room temperature), industrial viability and low-cost operation, environmentally friendly character. In addition, it offers the possibility of controlling the reduction reaction in both space and time, which helps regulating the growth of gold nanoparticle, their morphology (size and shape) and their dispersion in the reactive medium [31–34].

Thanks to its interesting physico-chemical features, ordered mesoporous silica (OMS) has been combined with gold nanoparticles in order to synthesize nanocomposites. OMS exhibits regular pores in terms of spatial arrangement and diameter, high specific surface areas and remarkable thermal stability as well as numerous silanol groups on their surface [35–39]. Several synthetic approaches of gold nanoparticles@OMS nanocomposites have been reported [40–44]. The incorporation of gold nanoparticles in the OMS structure is expected to produce a heterogeneous catalyst with high mechanical-thermal-chemical stability, high selectivity toward reactive molecules, high catalytic activity and potential recycling capacity [14,35–39,45]. The oxidation of

CO at low temperature by a gold-supported mesoporous silica catalyst described by Okumura *et al.* was reported [46]. The gold-based catalyst led to 50% conversion of CO at 227 K and exhibited a higher catalytic activity than gold catalysts supported either on TiO_2 or Al_2O_3. This result was confirmed by Daté *et al.* [47]. Gui *et al.* have developed gold nanoparticles@porous silica catalysts by an one-pot sol-gel method, exhibiting remarkable efficiency for the oxidation of cyclohexane [48]. Other studies about the reduction of *p*-nitro phenol into *p*-amino phenol have also evidenced the catalytic efficiency of gold-based silica catalysts [39,49].

The photogeneration of gold has been reported in functionalized ordered porous silicas. Fattori *et al.* have modified SBA-15 with 4,4'-bipyridinium functional groups before using it as a support for the photochemically-assisted formation of Au nanoparticles [50]. However, this approach has never been reported for pure silica OMS. Indeed, the main references found in the literature dealt with noble metals such as Ag and Pd nanoparticles confined in the OMS structures [51,52]. In the case of gold nanocomposites, the major silica supports studied are non-ordered porous silicas. The impregnation of a porous silica monolith with a solution gold salt followed by a photo-reduction process of at least 10 min has been reported for the production of Au nanoparticles in porous silica [53].

Herein, we present a simple method for generating gold@OMS nanocomposites via a photo-induced free-radical process. This synthesis involves a two-step procedure: in a first step, the SBA-15 type OMS support was prepared, then the gold cations underwent a photo-induced reduction. Several photonic and physicochemical parameters have been studied. The influence of gold precursor concentration, light intensity and nature of the solvents on nanoparticles formation (size, dispersion and stability) and their optical properties in the SBA-15 structure were thoroughly

analyzed. The catalytic performance has been evaluated with respect to the selective oxidation of benzyl alcohol in liquid phase.

2. Experimental section

2.1. Materials

For the synthesis of ordered mesoporous SBA-15 type material, the reagents used in the experiments were the triblock copolymer poly(ethylene glycol)-*block*-poly(propylene glycol)-*block*-poly(ethylene glycol), Pluronic® P-123 as the pore templating agent and tetraethyl orthosilicate (TEOS – 98%) as the silica source. Both were supplied by Sigma-Aldrich. Hydrochloric acid (37 wt.%) was purchased from Carlo Erba. For the photochemical synthesis, the metal precursor, gold tribromide ($AuBr_3 \geq 99.9\%$), was purchased from Sigma-Aldrich and the radical generator Irgacure 2959® (1-[4-(2-hydroxyethoxy) phenyl]-2-hydroxy-2methyl-1-propan-1-one) was purchased from BASF Chemical Co.

Prior to catalytic tests, analytical grade benzyl alcohol (named as BzOH, Fluka), benzaldehyde (BzCHO, Aldrich), benzoic acid (BzCOOH, Prolabo) and benzyl benzoate (BnBzO, Alfa Aesar) were used as calibration standards. For the catalytic tests, benzyl alcohol (Fluka), cyclohexane (Carlo Erba) and sodium carbonate (Fluka) were used as received.

2.2. Nanocomposite synthesis method

The non-aggregated SBA-15 micron-size particles were prepared according to the protocol described by Belmoujahid *et al.* [54], inspired by the original work of Zhao *et al.* [38] with slight modifications. The synthesis was performed with a molar ratio of 1 SiO_2 : 0.017 P123 : 5.68 HCl : 197 H_2O. After complete dissolution of P123 in HCl and distilled water heated at 40 °C, TEOS was added under stirring with a flow rate of 8 $mL.s^{-1}$. The mixture was left under static conditions

at 40 °C for a 2 h ageing step and then heated in a sealed flask at 90 °C for 24 h. The precipitated solid was recovered by filtration and washed with distilled water and then, dried for 12 h at 70 °C. Finally, the solid was calcined under air in a muffle furnace at 300 °C for 4 h (with a heating rate of 0.8 °C.min^{-1} from 20 to 300 °C) to remove the pore templating agent P123.

AuNPs@SBA-15 nanocomposites were prepared as follows: 15 mg of calcined SBA-15 was dispersed in 2 mL of solvent (distilled water or ethanol) in a 10 mL vial under magnetic stirring (450 rpm) during 20 min. An amount of x% $AuBr_3$ (where x represents the wt.% of $AuBr_3$: x = 0.25; 0.125; 0.05; 0.025 wt.%) was dissolved in this mixture, and then 0.5 wt.% of the free-radical generator Irgacure 2959 was added. After 1 h of magnetic stirring at 350 – 400 rpm in the dark, the colour of this formulation was orange or yellow, depending on the $AuBr_3$ concentration. Then, the formulation was immediately exposed to UV light in order to generate gold nanoparticles dispersed within the SBA-15 host. It is noteworthy that the silica support used was not previously functionalized. The photochemical reduction was performed with a 200 W Hg-Xe lamp – LC8-02A device from Hanamatsu. The experimental set up used to shape the actinic beam delivered a maximum fluence of 200 mW.cm^{-2} in the 300 – 450 nm range.

The irradiated solution was immediately analyzed by UV-Visible spectroscopy and then decanted in dark room for 12 h. The decanted solution was washed with distilled water and then, the solid phase recovered was dried at 70 °C during 24 h before TEM (Transmission Electron Microscopy), X-ray diffraction and N_2 adsorption / desorption manometry analyses.

2.3. Materials characterization

UV-Visible absorption spectroscopy (Thermo Fisher Scientific Evolution 201 spectrometer) was used to qualitatively establish the formation of gold nanoparticles.

Transmission Electron Microscopy (TEM) allowed to characterize the morphology and dispersion of gold nanoparticles in the support. Those experiments were carried out at 200 kV using a JEOL ARM 200 F instrument. The particles sizes distributions are determined from 200 particles using the Image J software.

X-ray powder diffraction (XRD) data were collected using a PANalytical X'Pert Pro diffractometer with a Cu anode operating at 50 kV/40 mA (λ = 0.15418 Å, 0.5° < 2θ < 10° and 2° < 2θ < 70°, 0.02 °.s^{-1}).

The textural properties of the materials were investigated using a Micromerictics Tristar instrument at -196 °C. The samples were out-gassed overnight under vacuum at 150 °C. The specific surface area was determined using the Brunauer – Emmett – Teller method in a relative pressure range of 0.05 to 0.35. The average pore diameter was determined using the Barrett – Joyner – Halenda (BJH) model applied to the desorption branch. The microporous volume was determined using the t-plot method.

Thermogravimetric Analysis (TGA), which allows quantifying the contents of physisorbed water, residual organic matter and silanol groups, was carried out on a TG METTLER TOLEDO STARe apparatus, under air flow, with a heating rate of 5 °C.min^{-1} from 30 to 800 °C.

X-ray photoelectron spectroscopy (XPS) analysis was performed on a VG Scienta (Uppsala, Sweden) SES 2002 X-ray photoelectron spectrometer under ultra-high vacuum (P < 10^{-9} mbar). The spectrometer resolution at the Fermi level is about 0.4 eV. The depth analyzed extends up to about 8 nm. The monochromatized Al Kα source (1486.6 eV) was operated at a power of 420 W (30 mA and 14 kV) and the spectra were acquired at a take-off angle of 90 ° (angle between the sample surface and photoemission direction). CASAXPS software (Casa Software Ltd, Teignmouth, UK, www.casaxps.com) was used for all peak fitting procedures. The intensity area

was determined using integrated peak areas of each component and taking into account the transmission factor of spectrometer, means free path, and sensibility factor of each atom.

2.4. Catalytic tests

The oxidation of benzyl alcohol was carried out in a 100 mL autoclave reactor (Parr) equipped with temperature and pressure controllers and external magnetic stirring (Figure A.1). In a typical experiment, benzyl alcohol (0.567g, 5 mmol), cyclohexane (solvent, 25 mL), AuNPs@SBA-15 catalyst (0.068g, BzOH:Au molar ratio 1530:1) and Na_2CO_3 (2.12g, BzOH: Na_2CO_3 molar ratio 1:4) were added to a glass vessel placed inside the stainless steel reactor. The latter was purged twice with pure O_2 and finally pressurized until 4 bar. The mixture was heated gradually and stirred at 500 rpm during the whole experiment. The reaction started (t = 0) when the temperature was reached (100 or 130 ºC, respectively). After 1 or 4 h, respectively, the reactor was cooled down in an ice bath, depressurized and opened to withdraw a sample. Samples were microfiltered, diluted in ethanol and analyzed in an Agilent 6890N GC system equipped with Solgel-Wax capillary column.

The stability was studied in the spent samples recovered from post-reaction mixture. In order to isolate the catalyst from the heterogeneous (completely insoluble) base, Na_2CO_3 was extracted and dissolved in water. The solid catalyst was then filtered, washed with water and dried overnight at 110 ºC. BzOH:Au:Na_2CO_3 molar ratio were kept constant during all the experiments. The conversion and selectivity values were calculated according to Equations 1 and 2.

$$Conversion\ (\%) = \frac{(n\ BzOH)_{initial} - (n\ BzOH)_{final}}{(n\ BzOH)_{initial}} \times 100 \qquad \text{Eq. 1.}$$

$$Selectivity\ (\%)_{BzCHO} = \frac{(n\ BzOH)}{\Sigma\ (n\ BzCHO + n\ BzCOOH + n\ BnBzOH)} \times 100 \qquad \text{Eq. 2.}$$

3. Results and discussion

3.1. Photoinduced generation of size-controlled gold nanoparticles

In order to obtain a gold@SBA-15 nanocomposite, gold nanoparticles were synthesized *in situ* by using distilled water and ethanol as solvents. Preliminary studies with ethanol as a solvent, aimed at determining the influence of photonic parameters on the formation and optical properties of gold nanoparticles (AuNPs). The photonic conditions were defined as follows: light intensity 50 $mW.cm^{-2}$ with a 4 min exposure.

Before and after irradiation the formulations were analyzed by UV-Vis spectrophotometry (Figure 1). In their initial state, ethanol or water solutions of $AuBr_3$ exhibited an orange brown colour with an absorption band around 380 nm [55]. After irradiation, the UV-Vis spectra showed the presence of a new band for both solvents (at 540 nm in ethanol and 527 nm in H_2O) with a red purple colour, which is characteristic of the presence of gold nanoparticles [56,57]. At the same time, in both formulations, the characteristic band of gold cations at 380 – 385 nm was no longer visible at the end of the irradiation, thus indicating the reduction of Au^{3+} species to Au^0.

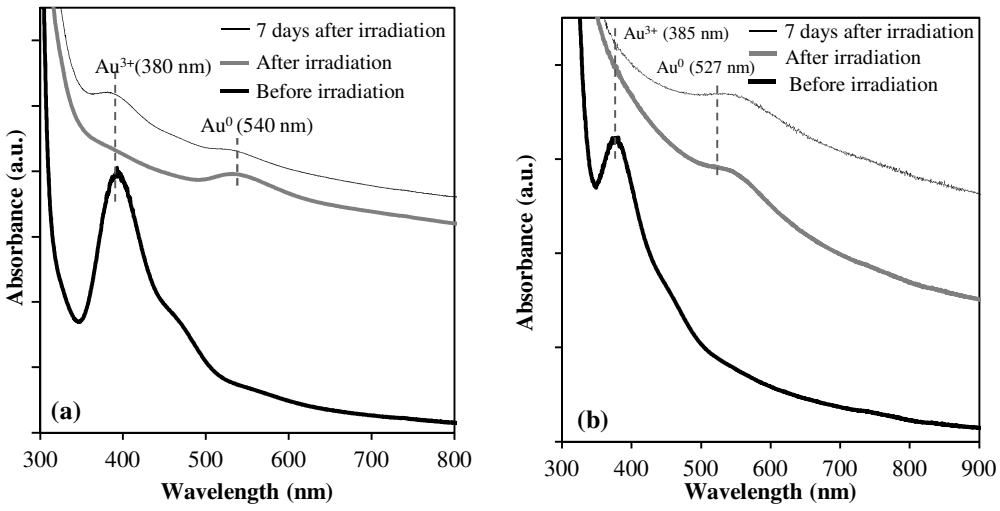

Figure 1. UV-visible absorption spectra of formulations prepared in (a) ethanol and (b) water.

In order to determine the influence of the solvent on the synthesis of Au nanoparticles, and more particularly on the optical properties of AuNPs formed on the structure of the SBA-15 support, the stability of as-prepared nanoparticles after irradiation in ethanol and water was studied. The two formulations were stored in the dark for 7 days. In the case of ethanol, after ageing for 7 days, the colour of the formulation turned from red-purple to brown while a new absorption band emerged in the UV-Visible spectrum at 380 nm with a concomitant decrease of the band at 540 nm [58]. This result indicates the instability of Au^0 particles in ethanol.

On the other hand, the AuNPs in water exhibited a fair stability over the same period. The colour of the formulation and the absorption band at 527 nm did not change over a 7 days storage period (Figure 1). Because of the remarkable stability of the gold@SBA-15 nanocomposite synthesized in water, this solvent was used in the forthcoming experiments presented in this work.

The colour changes of the solutions are summarized in Table A.1.

Then, the influence of the concentration of metal precursor was studied in H_2O and under the same photonic conditions (50 mW/cm^2 and 4 min UV-exposure). The colour of the solution varied from orange to yellow, then light yellow, showing the decrease in cations concentration and also the conversion of Au^{3+} to Au^{2+} and Au^{+} (see Table A.2) [59]. The colour of the solution after the irradiation turned from purple to pink with a decrease in Au concentration, attributed to the presumed formation of smaller AuNPs.

The UV-visible spectra before and after irradiation for decreasing Au^{3+} concentrations are shown in Figure 2. The position of the absorption band assigned to AuNPs was blue-shifted from 585 nm to 520 nm, as the gold precursor concentration diminished. The shift of the band to lower wavelengths indicates a decrease of the size of gold nanoparticles.

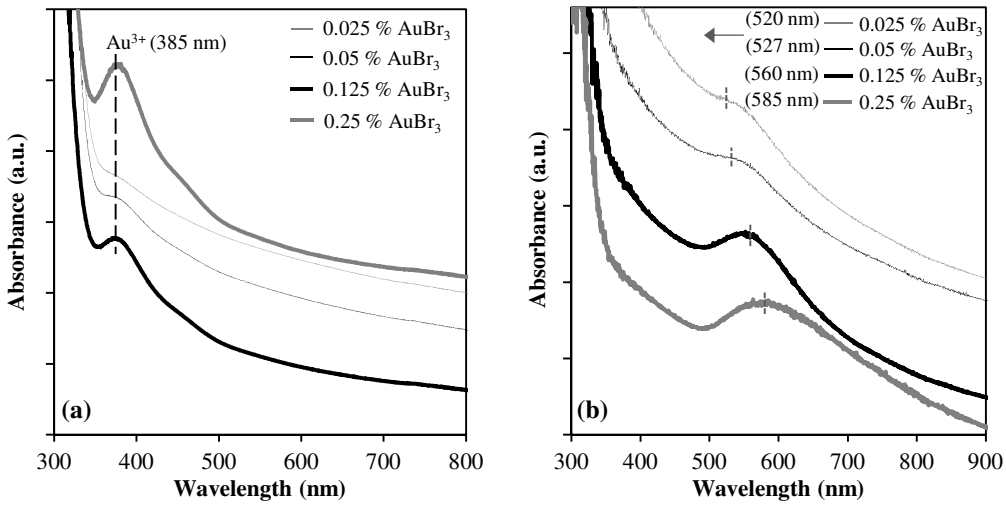

Figure 2. UV-visible absorption spectra of formulations in water medium (a) before and (b) after the irradiation as a function of gold salt concentration.

With a view to improve the characterization of as-developed nanomaterials, TEM observations of this nanocomposite (Figure 3) were performed in order to determine the size and dispersion of gold nanoparticles within SBA-15 support as a function of their concentrations. The TEM images illustrate the presence of spherical particles covering the SBA-15 support. The size of the nanoparticles was observed to decrease while diminishing the metal precursor concentration [60,61]. Indeed, the size, the concentration and the aggregation level of gold nanoparticles are very important according to the different applications. It has been demonstrated, according to Mie theory, that the higher the initial concentration of gold is, the larger the size of the nanoparticles becomes. In the case of 0.25 and 0.125 wt.% $AuBr_3$ samples, the AuNPs were found to be large and probably localized at the external surface of the SBA-15 support. The size measured by TEM was 29.9 ± 3 nm and 15 ± 2 nm, respectively; some aggregates were also visible (Figures 3a and 3b). In contrast, samples containing 0.05 and 0.025 wt.% $AuBr_3$ led to smaller and well dispersed nanoparticles formation with a narrow size distribution (Figures 3c and 3d). Their average size was measured to be 6.0 ± 0.5 nm and 4.9 ± 0.5 nm, respectively.

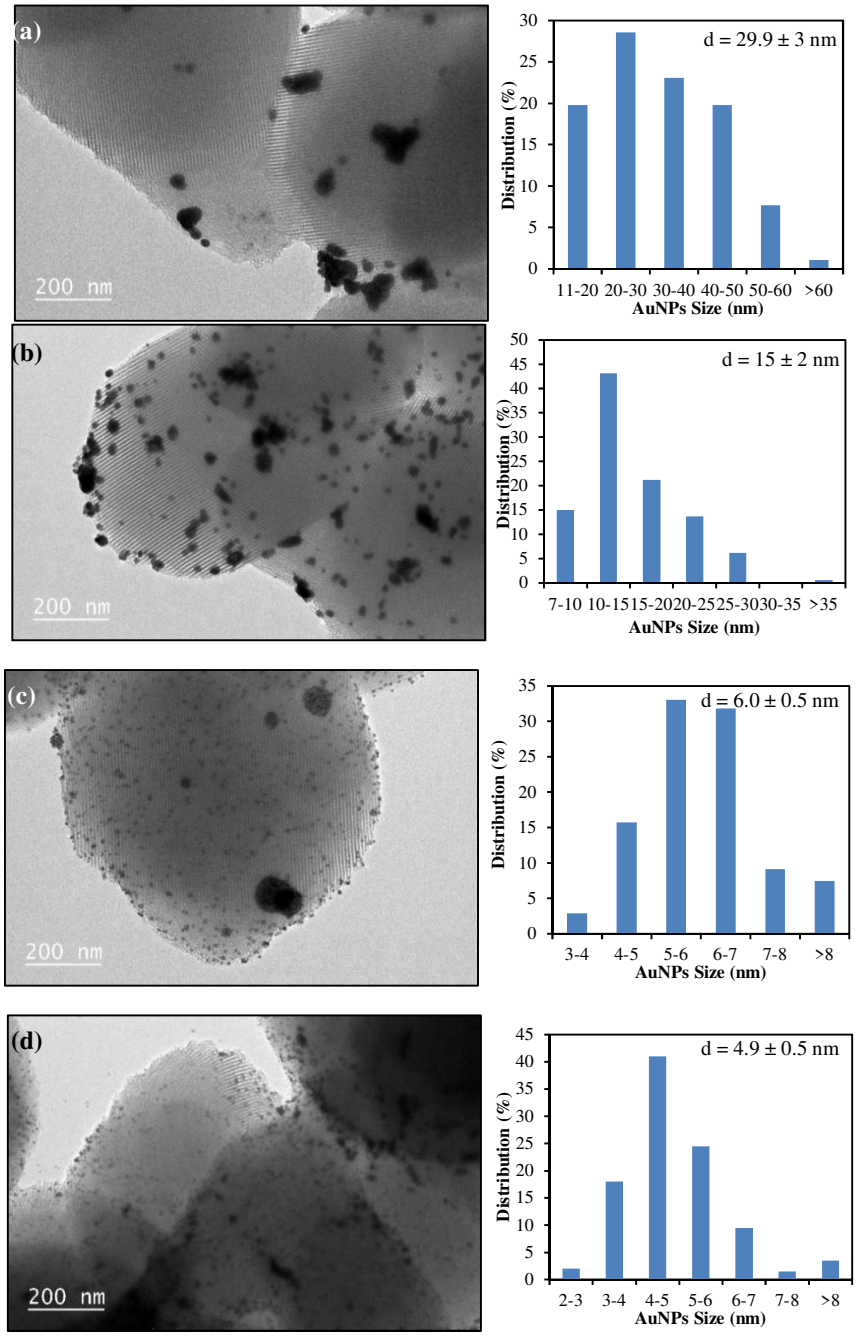

Figure 3. TEM images of AuNPs@SBA-15 nanocomposites and AuNPs size distributions as a function of the gold salt concentration:(a) 0.25 %, (b) 0.125 %, (c) 0.05 % and (d) 0.025 % $AuBr_3$.

It is important to notice that they are in the same range in size as the internal mesopore diameter of the host (see Table 1), which means that AuNPs can be located both at the external surface and

inside the mesopores. Therefore, in-depth characterizations were performed to determine the position of AuNPs on the 0.05 wt.% AuNPs@SBA-15 nanocomposite which should contain a large amount of gold. For the following of the study, this concentration was used and referred to AuNPs@SBA-15.

3.2. In-depth characterization of the AuNPs@SBA-15 nanocomposite

In order to determine its physico-chemical properties, the optimized AuNPs@SBA-15 nanocomposite was characterized by TEM, XRD and nitrogen physisorption manometry techniques.

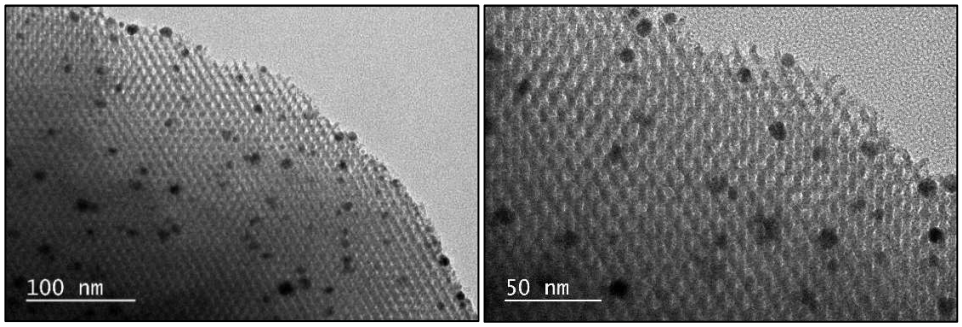

Figure 4. TEM images at different scales of the optimized nanocomposites AuNPs@SBA-15.

TEM images shown in Figure 4 reveal that the nanoparticles are spherical with an average narrow diameter of 6.0 ± 0.5 nm, and are well dispersed within the mesoporous structure or on the surface of the silica host. Only few aggregates are visible. 3D TEM tomography experiments performed on the optimized nanocomposite AuNPs@SBA-15 (not presented here) indicated that the AuNPs are localized near the surface of SBA-15 particles. The AuNPs have probably grown at the entrance of the pores since their size matches with that of the pores. This is probably due to preferential adsorption of Au salts at the surface of SBA-15 particles.

The low and wide angles XRD patterns of the nanocomposite are presented in Figure 5. At low angles (Figure 5a), the composite as well as the SBA-15 host support, exhibit three diffraction

peaks corresponding to (100), (110) and (200) reflection plans characteristic of a 2D hexagonal *P6mm* symmetry. In order to study the impact of the UV-treatment on the structural and textural properties of the SiO_2 network, the SBA-15 host has been treated under the same conditions: dispersion in H_2O and exposure to UV-light for 4 min. Likewise, the SBA-15 was also dispersed in water without irradiation as a blank experiment.

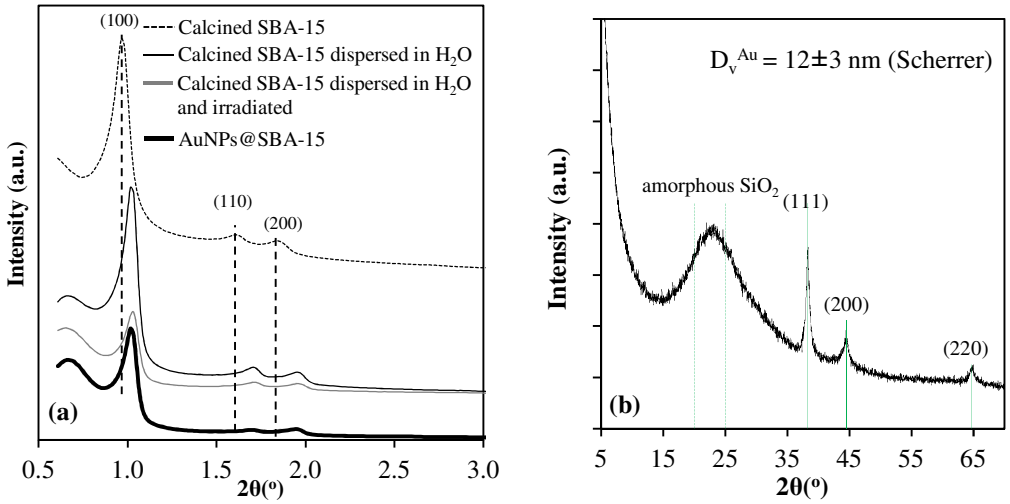

Figure 5. Powder X-ray diffraction patterns (a) at low angles of different SBA-15 samples and the optimized AuNPs@SBA-15 and (b) at wide angles of the AuNPs@SBA-15 nanocomposite.

The peak positions of the 3 SBA-15 samples dispersed in H_2O with and without UV-exposure and the AuNPs@SBA-15 shifted slightly; so, their lattice parameter shows only a slight decrease compared to pristine SBA-15. This indicates a contraction of the porous network upon dispersion in H_2O and subsequent drying. Indeed, the pore network contraction is similar for the 3 samples, which indicates that the photochemical treatment has no influence on the structural organisation of the composite.

At wide angles, the XRD pattern of the AuNPs@SBA-15 nanocomposite (Figure 5b) confirms the formation of Au^0 nanoparticles since 3 broad peaks in the range 30 – 70 °2θ corresponding to (110), (200) and (220) reflection planes of crystalline gold were observed. According to Scherrer

equation, the average gold crystal size can be estimated to 12 ± 3 nm. This XRD estimation suggests the presence of larger particles compared to TEM observations, which can be explained by the presence of aggregated Au particles on the surface of SBA-15 that are taken into account when particle size is calculated using the Scherrer equation. Hence, this contributes to increase the average particle size. The broad peak at 20 – 25 °θ is characteristic of the amorphous SBA-15 silica framework.

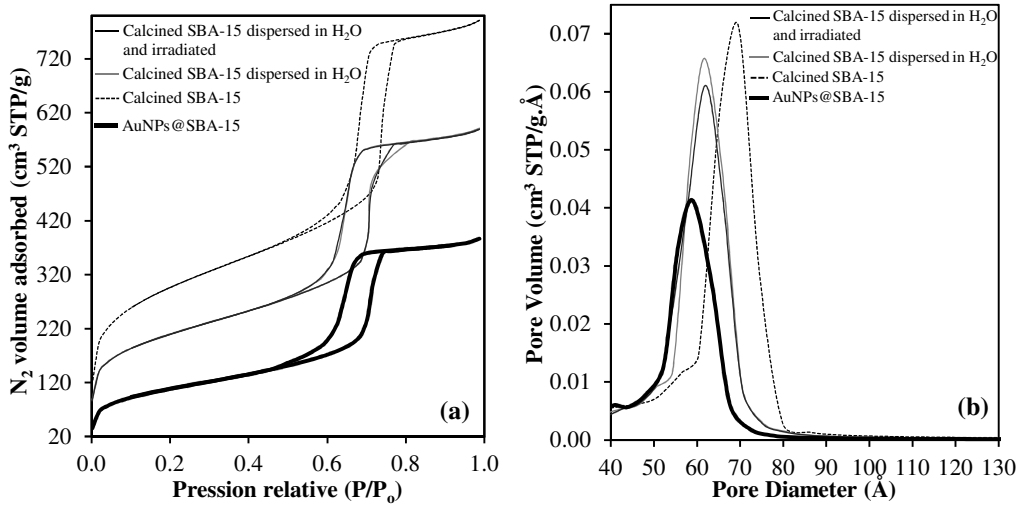

Figure 6. (a) Nitrogen sorption isotherms and (b) pore size distributions of different SBA-15 samples and optimized AuNPs@SBA-15.

The textural properties of the SBA-15 host and AuNPs@SBA-15 were studied by nitrogen adsorption / desorption. According to IUPAC classification, pristine SBA-15 support and AuNPs@SBA-15 nanocomposite exhibit type IV isotherm with a H1 hysteresis, which is characteristic of mesoporous materials (Figure 6). However, the textural parameters (specific surface area and pore volume) of the nanocomposite are lower than those of the SBA-15 pristine host silica (Table 1). Although the nanocomposite still exhibits a high specific surface area (392 m^2/g) and a high pore volume (0.57 cm^3/g), relative to the parent silica, there is a loss of 63 % of the specific surface area and of 50 % of the pore volume.

Table 1. Textural parameters of different SBA-15 samples and optimized AuNPs@SBA-15

Samples / Textural parameters		calcined SBA-15	calcined SBA-15 dispersed in H_2O	calcined SBA-15 dispersed in H_2O and irradiated	AuNPs@SBA-15
BET specific surface area (m^2/g)		**1069**	**746**	**746**	**392**
Volume (cm^3/g)	Total pore	1.2	0.9	0.9	0.57
	Micropore	0.2	0.1	0.1	0.02
	Mesopore	1.0	0.8	0.8	0.55
Average BJH pore diameter (nm)		**6.8 – 7.0**	**6.0 – 6.2**	**6.0 – 6.2**	**5.8 – 6.2**

This can be explained first by the preparation of the nanocomposite using water as a solvent. Indeed, for the SBA-15 dispersed in H_2O, the loss of specific surface area is 48 % (instead of 63 %) and the loss of pore volume is of 37 % (instead of 50 %). As observed by XRD (Figure 5a), the dispersion in water and subsequent drying have an impact on the structure and therefore on the porous texture of the nanocomposite. On the other hand, since the irradiation has no influence on the mesostructure, it has therefore no influence on the textural parameters (see textural parameters of SBA-15 dispersed in H_2O and SBA-15 dispersed in H_2O and irradiated reported in Table 1 and Figure 6). It should be noticed that the AuNPs@SBA-15 nanocomposite did not exhibit micropores, which explains the low specific surface area and pore volume. This can be explained by the obstruction of the SBA-15 micropores by residual organic matter from the 1-[4-(2-hydroxyethoxy) phenyl]-2-hydroxy-2-methyl-1-propan-1-one used as the radical generator.

The optimized AuNPs@SBA-15 nanocomposite was analyzed by thermogravimetry and compared to the calcined SBA-15 support as presented in Figure 7.

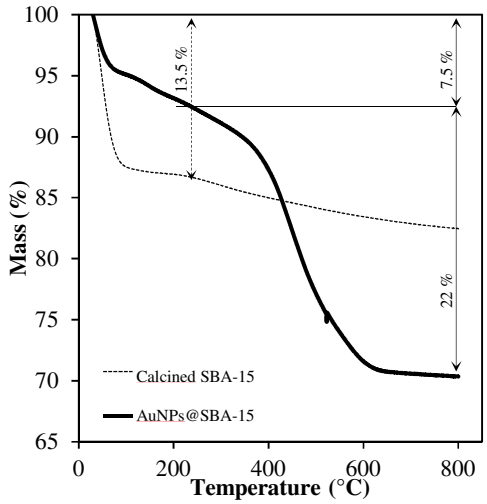

Figure 7. Thermogravimetric analysis of calcined SBA-15 and optimized AuNPs@SBA-15.

A first loss of mass of 13.5 % for calcined SBA-15 and 7.5 % for AuNPs@SBA-15 nanocomposite was observed from 25 to 220 °C, respectively. This mass loss corresponds to the release of physisorbed water from the material in both cases. The greater amount of physisorbed water on calcined SBA-15 can be assigned to a high silanol content generally observed on SBA-15 calcined at 300 °C. The second mass loss of 4 % observed from 220 to 800 °C for calcined SBA-15 can be explained by the condensation of silanols upon increasing the temperature.

A 22 % weight loss has also been observed for this nanocomposite beyond 220 °C. It can be assumed that this mass loss corresponds mainly to the oxidation of the residues from the radical generator. The washing protocol performed after the photo-reduction reaction probably only partially removed those residues. The presence of this organic matter may also explain the greater decrease of the textural parameters.

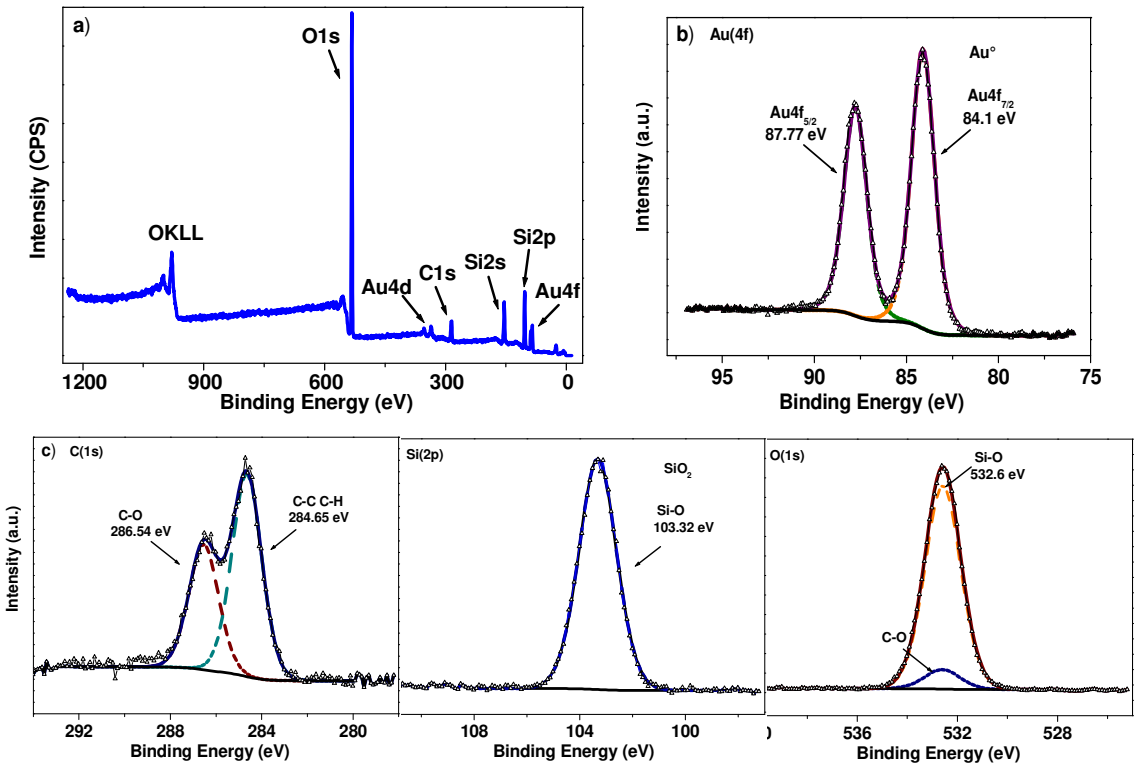

Figure 8. a) XPS survey spectrum of the optimized AuNPs@SBA-15 nanocomposite; XPS spectra of b) Au4f 7/2 of the sample after 4 min UV-exposure c) C, Si and O.

XPS analysis was carried out to study the surface chemistry of AuNPs@SBA-15 nanocomposite (composition and structure). As it can be seen in Figure 8a and Table 2, Si, C, O and Au are the main elements found from the survey spectra of the nanocomposite materials. No trace of Br is detected meaning that Br is release in solution.

Table 2. XPS results of optimized AuNPs@SBA-15

Block Id	Name	Position	%At Conc.
Au 4f	Au 4f 7/2 Au^0	84.10	0.94
C 1s	C-C C-H	284.65	9.00
C 1s	C-O	286.54	5.56
O 1s	Si-O C-O	532.60	57.23

Si 2p	Si-O	103.32	27.27

This is consistent with the chemical components of the SBA-15 host and Au stemming from the photo-reduction of Au^{3+} cations. A percentage of 0.94 %at of Au has been determined here. For catalytic tests a 0.94 wt.% of Au has been used. The energy spectrum of Au 4f 7/2 (84.10 ± 0.1 eV) is reported in Figure 8b the position of the peak corresponds to Au^0 [62]. The change in the corresponding Au 4f 7/2 from Au^{3+} peak (85.5 ± 0.3 eV) [63–65] to binding energies 84.10 eV was linked to the reduction of Au^{3+} into AuNPs. Since no other form of Au is visible, the reduction of Au^{3+} can be postulated as complete. In stark contrast to what can be found in the literature, Au nanoparticles generated according to this procedure do not contain any covalently bound stabilizers. However, the substituted benzoyl radicals resulting from the cleavage reaction of Irgacure 2959, which are known to oxidize to carboxylic acid, might interact mildly with the nanoparticles [33,66]. In addition, the presence of a large amount of carbon confirms the presence of residual organic matter that probably obstructs the microporosity and part of the mesoporosity.

3.3. Catalytic study

The catalytic performance of optimized AuNPs@SBA-15 sample was evaluated in the selective oxidation of benzyl alcohol under oxygen atmosphere. The reaction conditions were chosen on the basis of previous literature reports [11–13,67,68]. It is well known that gold activity strongly depends on both oxygen concentration (pressure) and the presence of base as co-catalyst [69–71]. However, the use of strong bases as NaOH usually leads to the consecutive oxidation of the alcohol function to the corresponding carboxylic acid *i.e.* benzoic acid, which diminishes therefore the selectivity towards benzaldehyde [68]**.** According to Ferraz *et al.* [68], the use of weak bases such as K_2CO_3 may favor the selectivity in benzaldehyde. One may therefore expect to achieve good

conversion and selectivity values under 5 bar oxygen pressure. Besides, the presence of non-aqueous solvents as cyclohexane, inhibits somehow the total oxidation of the alcohol, being also beneficial in comparison with the solvent-free oxidation of benzyl alcohol [68].

Table 3 summarizes conversion and selectivity values obtained over the optimized AuNPs@SBA-15 sample at different temperatures and reaction times. As expected, benzyl alcohol conversion increases with reaction time and temperature, which also affects the selectivity. Conversion values obtained at 100 and 130 °C after 1 h are rather similar (entries 1 and 3). However, the selectivity towards benzaldehyde raises (+ 24%) at 130 ºC. Differences are more significant after 4 h (entries 2 and 4), the conversion doubled at 130 ºC, with a 91% selectivity to benzaldehyde. It should be noted that the selectivity towards BzCOOH is 0% in all experiments, only BnBzOH and BzCHO have been detected as products. This accounts for the fast condensation of BzCOOH and BzOH under the selected reaction conditions (Scheme A.1). Anyway, the observed values are comparable with those reported in the literature for gold supported on different oxides under similar reaction conditions [67,68]. In order to facilitate a proper comparison with the reported data, specific activity (SA = $\frac{mole\ BzOH\ converted}{mole\ Au*s*g\ catalyst}$) and turn-over-frequency (TOF) values (TOF = $\frac{mole\ BzOH\ converted}{mole\ Au*h*dispersion}$) has been calculated taking into account the real Au contents measured from ICP and the gold dispersion estimated from the average gold particle size deduced from TEM and mathematically modeled for cuboctahedral particles [72]. As expected, due to the endothermic character of the reaction, both specific activity and TOF increase with the temperature. The obtained TOF values are comparable (Table 3, entry 1) or even higher (Table 3, entry 3) than those previously reported for different supports including gallia, ceria and titania under solvent-free conditions, thus pointing out the suitability of the prepared material for the oxidation process [67].

Table 3. Influence of reaction time and temperature over optimized AuNPs@SBA-15

Entry	Temperature (ºC)	Time (h)	Conversion (%)	Selectivity (%)			Specific activity ($s.g^{-1}$)	TOF (h^{-1})
				BzCHO	BzCOOH	BnBzO		
1	100	1	12	56	0	44	0.243	482
2		4	26	77	0	23	-	-
3	130	1	17	80	0	20	0.345	684
4		4	51	91	0	9	-	-

Reaction conditions: BzOH (0.5667 g, 5 mmol), cyclohexane (25 mL), catalyst (68.2 mg, BzOH:Au molar ratio 1530:1) and Na_2CO_3 (2.12 g, BzOH:Na_2CO_3 molar ratio 1:4). Temperature was set at 100 or 130 ºC, respectively, O_2 pressure at 4 bars and stirring rate at 500 rpm.

The influence of BzOH : Au molar ratio at different reaction times was also studied at 130 ºC (Table 4). Logically, the activity increases with BzOH : Au molar ratio due to the greater availability of AuNPs to interact with benzyl alcohol molecules. Similar data can be obtained after 4 h at a ratio of 1530 : 1 (entry 2) and 1 h at a ratio of 400 : 1 (entry 3). A remarkable conversion (71%) and selectivity in BzCHO (92%) were achieved after a reaction time of 4 h as well as a remarkable TOF (Table 4, entry 3) which doubles those values reported elsewhere [67].

Table 4. Influence of BzOH : Au molar ratio over optimized AuNPs@SBA-15

Entry				Selectivity (%)		

	BzOH : Au molar ratio	Time (h)	Conversion (%)	BzCHO	BzCOOH	BnBzO	Specific activity ($s.g^{-1}$)	TOF (h^{-1})
1	1530:1	1	17	80	0	20	0.345	684
2		4	51	91	0	9	-	-
3	400:1	1	51	90	0	10	0.4	1,267
4		4	71	92	0	8	-	-

Reaction conditions: BzOH (0.5667 g, 5 mmol), cyclohexane (25 mL), catalyst (68.2 mg / 110 mg, respectively, BzOH:Au molar ratio of 1530:1 / 400:1, respectively) and Na_2CO_3 (2.12 g, BzOH: Na_2CO_3 molar ratio 1:4). Temperature was set at 130 ºC, O_2 pressure at 4 bars and stirring rate at 500 rpm.

The possibility of recycling the catalyst was also evaluated by reusing the spent catalyst for 4 cycles at 130 °C (Table 5). Surprisingly, the conversion increased by 15% during the second run, while maintaining the same selectivity. According to the results obtained by TGA and XPS analyzes, some organics remain in the fresh catalyst after washing, which could hinder the interaction of the alcohol molecule at the surface of gold. After the first run, these residual organic compounds can be partially removed, which would lead to a better BzOH-Au interaction during the second catalytic run and, therefore, to a higher conversion.

Table 5. Recycling study over optimized AuNPs@SBA-15 catalyst

#Run	Conversion (%)	Selectivity (%)		
		BzCHO	BzCOOH	BnBzO
1	51	90	0	10
2	66	90	0	10
3	24	82	0	18
4	36	84	0	16

Reaction conditions: BzOH (0.5667 g, 5 mmol), cyclohexane (25 mL), catalyst (68.2 mg, BzOH:Au molar ratio of 400:1) and Na_2CO_3 (2.12 g, BzOH: Na_2CO_3 molar ratio 1:4). Temperature was set at 130 ºC, O_2 pressure at 4 bar and stirring rate at 500 rpm. Molar ratios were kept constant during all runs.

Catalyst activity drops to 24% BzOH conversion in the 3rd run and again increases to 36% after the 4th cycle. Although these values may appear contradictory, they can be understood when integrating with experimental details. The drop in conversion after the 3rd cycle could be expected, since leaching and sintering of gold are very common in liquid-phase reactions [73]. However, the strong adsorption of carboxylic compounds on the gold surface has been also extensively reported as one of the main causes of deactivation during recycling [74,75]. Hence, it can be expected that a combination of different causes may induce a fall of the activity after the 3rd cycle. Both the sintering and leaching processes are irreversible. However, the harmful adsorption of reaction intermediates at the catalyst surface can be overcome in some cases with a proper washing protocol after recover and before reuse. For this purpose, the post 3rd run catalyst was recovered and isolated by extraction with water. Once sodium carbonate is completely dissolved, the mixture is stirred for 5 min in order to clean the surface of gold by sodium benzoate as previously reported for similar systems [69]. After filtration and drying overnight, the post 3rd run catalyst was used for a 4th run (entry 4, table 5). The conversion increases by 12% from the 3rd run to the 4th run, the selectivity values remaining very similar. The latter reinforces the idea that reaction intermediates could be poisoning by adsorption the surface of gold particles. However, TEM observations of the gold catalyst after the liquid-phase reaction (run 2, 3 and 4) also showed that gold nanoparticles have coalesced and that the mesostructure of the support has been strongly modified to become macroporous with regular pore size while the particle morphology remained the same (Figure 9).

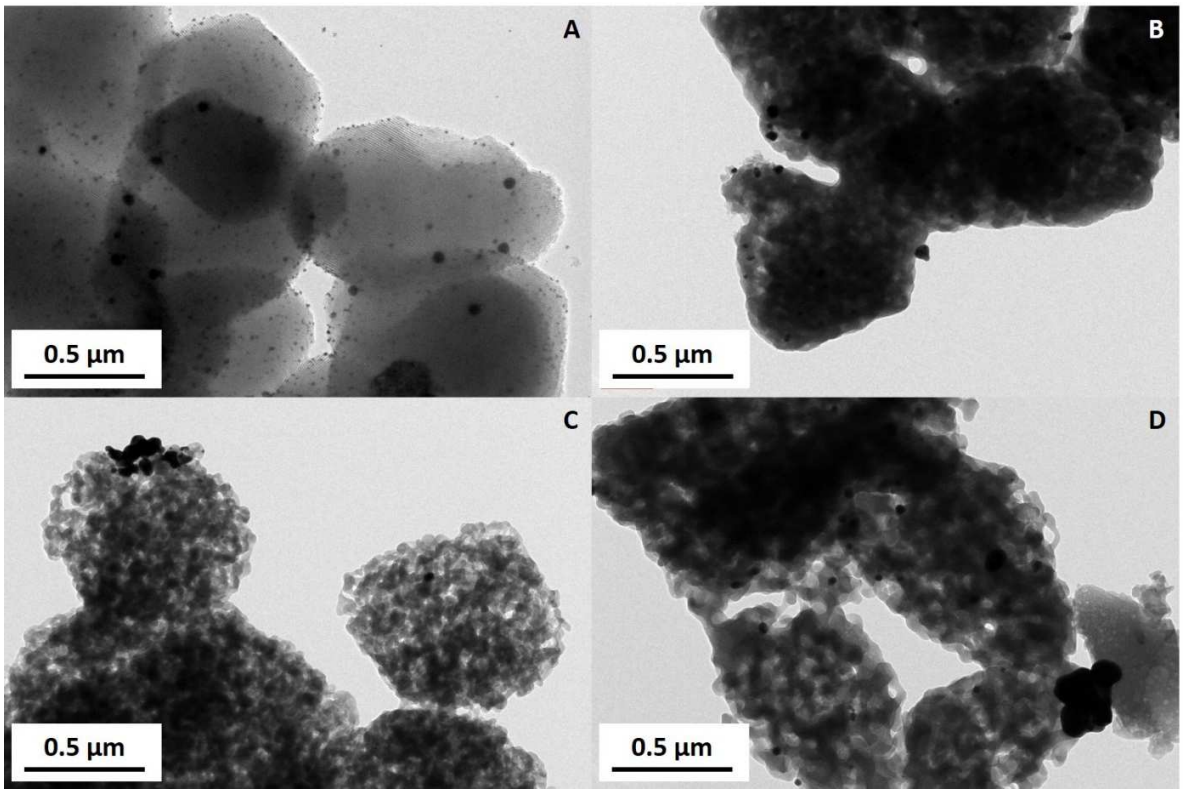

Figure 9. TEM images of (A) the fresh AuNPs@SBA-15 catalyst and the spent AuNPs@SBA-15 catalyst after (B) 2nd, (C) 3rd and (D) 4th run.

The coalescence observed on TEM images is confirmed by XPS analysis of the catalyst after reaction. Indeed, Si, C, O and Au are still the main elements found from the survey spectra of the nanocomposites materials (Figure 10a). The energy spectrum of Au 4f 7/2 (84.20 ± 0.1 eV) is reported in Figure 10b. The position of the peak corresponds to Au^0 and there is no change from the spectrum of the fresh catalyst where AuNPs are still present.

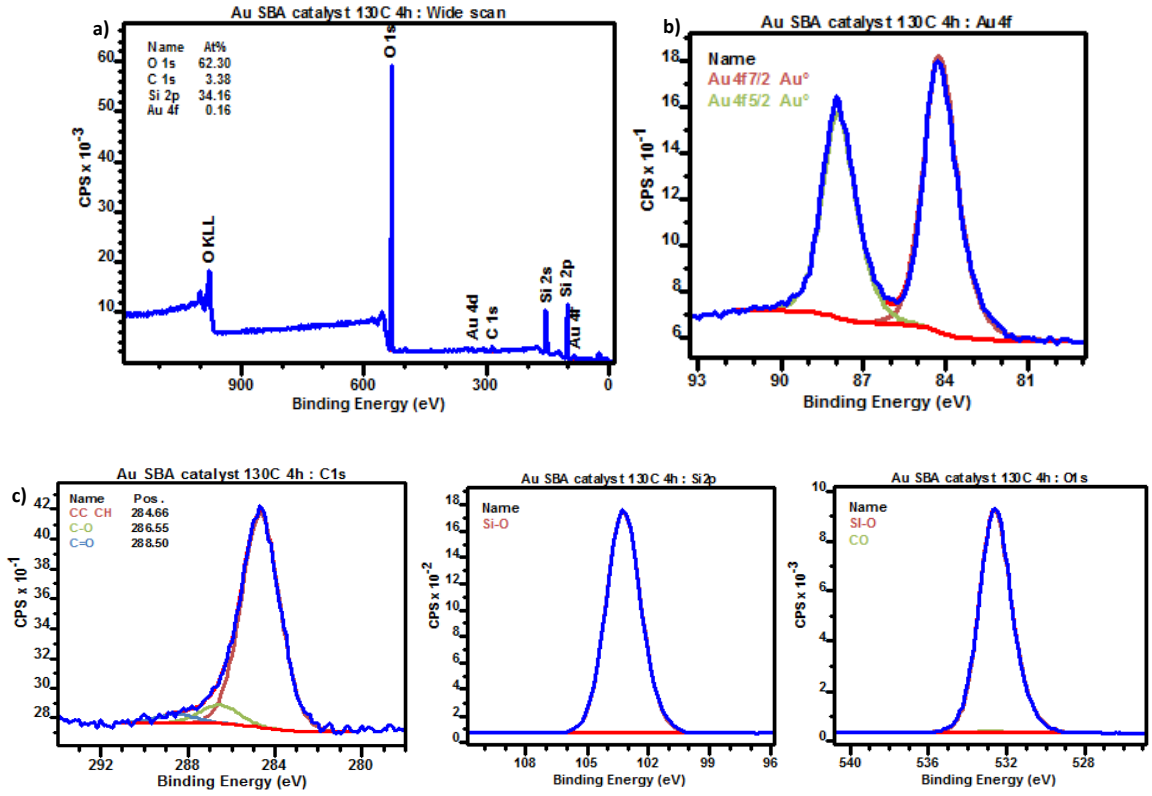

Figure 10. a) XPS survey spectrum of the spent AuNPs@SBA-15 catalyst after 4th run at the reaction conditions of temperature 130 ºC and time 4 h; XPS spectra of b) Au4f 7/2 c) C, Si and O of this sample.

A quantity of 0.17 %at of Au has been determined after reaction in opposition to 0.94 %at before reaction (Table 6). Such decrease is probably not due to a loss of gold nanoparticles during the catalytic reaction, but rather to the sintering process of the nanoparticles as shown by TEM (Figure 9).

Table 6. XPS results of the spent AuNPs@SBA-15 catalyst after 4th run at the reaction conditions of temperature 130 ºC and time 4 h

Block Id	Name	Position	%At Conc.
Au 4f	Au 4f 7/2 Au0	84.20	0.17

C 1s	C-C C-H	284.66	2.95
C 1s	C-O	286.55	0.26
O 1s	Si-O C-O	532.57	62.10
Si 2p	Si-O	103.25	34.39

4. Conclusions

In this study, a photochemical approach has been developed to produce AuNP@SBA-15 nanocomposites using green solvent. Different gold precursor concentrations ranging from 0.025 to 0.25%, light intensity and solvents have been studied in order to obtain gold nanoparticles with controlled size, well dispersed on an SBA-15 type ordered mesoporous silica surface. A concentration of 0.05 % of gold precursor, with a light intensity 50 mW/cm^2 with an exposure time of 4 min allowed to obtain a nanocomposite which exhibits an average gold nanoparticles size of 6.0 ± 0.5 nm on the mesoporous support where the structure and texture of the host matrix is maintained after irradiation.

The method developed herein is fast, simple to implement and based on water as a solvent. TEM, XRD and XPS studies confirmed the possibility of photochemically producing a new nanocomposite while controlling the size and insuring an excellent dispersion of the photogenerated spherical nanoparticles on SBA-15 host surface.

The catalytic performance of the optimized AuNPs@SBA-15 sample was evaluated in the selective oxidation of benzyl alcohol under oxygen atmosphere. Remarkable conversion (71%) and BzCHO selectivity (92%) was observed after 4 h reaction time, which makes AuNPs@SBA-15 very promising catalysts under the reaction conditions prevailing in this study. The catalyst has

been recycled and reused; however, the TEM observations after 4 cycles showed that gold nanoparticles have a tendency towards coalescence.

Appendices

The following file is available free of charge in the supplementary information file:

Scheme A.1. General reaction network involving benzyl alcohol conversion

Figure A.1. High-pressure device used for catalytic tests.

Table A.1. Experimental conditions of photochemical treatments in ethanol and water mediums and visual observations over time

Table A.2. Experimental conditions of photochemical treatments in water mediums on formulations of different gold salt concentrations and visual observations

Abbreviations

AuNPs: gold nanoparticles, AuNPs@SBA-15: nanocomposites of gold nanoparticles on mesoporous silica of type SBA-15, BzOH: benzyl alcohol, BzCHO: benzaldehyde, BzCOOH: benzoic acid and BnBzO: benzyl benzoate, EtOH: ethanol.

Acknowledgment

The authors would like to thank the “adsorption”, “X-ray diffusion” and “electronic microscopy” platforms of IS2M.

References

[1] P.H.C. Camargo, K.G. Satyanarayana, F. Wypych, Nanocomposites: synthesis, structure, properties and new application opportunities, Mater. Res. 12 (2009) 1–39. doi:10.1590/S1516-14392009000100002.
[2] S. Cheng, Y. Wei, Q. Feng, K.-Y. Qiu, J.-B. Pang, S.A. Jansen, R. Yin, K. Ong, Facile Synthesis of Mesoporous Gold−Silica Nanocomposite Materials via Sol−Gel Process with Nonsurfactant Templates, Chem. Mater. 15 (2003) 1560–1566. doi:10.1021/cm0202106.
[3] K. Mallick, M.J. Witcomb, M.S. Scurrell, Polyaniline stabilized highly dispersed gold nanoparticle: an in-situ chemical synthesis route, J. Mater. Sci. 41 (2006) 6189–6192. doi:10.1007/s10853-006-0019-6.
[4] B.K. Min, C.M. Friend, Heterogeneous Gold-Based Catalysis for Green Chemistry: Low-Temperature CO Oxidation and Propene Oxidation, Chem. Rev. 107 (2007) 2709–2724. doi:10.1021/cr050954d.
[5] Z. Hao, D. Cheng, Y. Guo, Y. Liang, Supported gold catalysts used for ozone decomposition and simultaneous elimination of ozone and carbon monoxide at ambient temperature, Appl. Catal. B Environ. 33 (2001) 217–222. doi:10.1016/S0926-3373(01)00172-2.
[6] S. Minicò, S. Scirè, C. Crisafulli, S. Galvagno, Influence of catalyst pretreatments on volatile organic compounds oxidation over gold/iron oxide, Appl. Catal. B Environ. 34 (2001) 277–285. doi:10.1016/S0926-3373(01)00221-1.
[7] M.P. de Almeida, S.A.C. Carabineiro, Dioxin Decomposition and Detection Using Gold Based Materials, Recent Pat. Chem. Eng. 5 (2012) 56–62. doi:10.2174/2211334711205010056.
[8] C. Megías-Sayago, S. Ivanova, C. López-Cartes, M.A. Centeno, J.A. Odriozola, Gold catalysts screening in base-free aerobic oxidation of glucose to gluconic acid, Catal. Today. 279 (2017) 148–154. doi:10.1016/j.cattod.2016.06.046.
[9] C. Megías-Sayago, K. Chakarova, A. Penkova, A. Lolli, S. Ivanova, S. Albonetti, F. Cavani, J.A. Odriozola, Understanding the Role of the Acid Sites in 5-Hydroxymethylfurfural Oxidation to 2,5-Furandicarboxylic Acid Reaction over Gold Catalysts: Surface Investigation on $Ce_xZr_{1-x}O_2$ Compounds, ACS Catal. 8 (2018) 11154–11164. doi:10.1021/acscatal.8b02522.
[10] M. Hudlicky, Oxidations in organic chemistry, American Chemical Society, Washington, DC, 1990.
[11] C.Y. Ma, B.J. Dou, J.J. Li, J. Cheng, Q. Hu, Z.P. Hao, S.Z. Qiao, Catalytic oxidation of benzyl alcohol on Au or Au–Pd nanoparticles confined in mesoporous silica, Appl. Catal. B Environ. 92 (2009) 202–208. doi:10.1016/j.apcatb.2009.07.007.
[12] J. Sun, Y. Han, H. Fu, X. Qu, Z. Xu, S. Zheng, Au@Pd/TiO_2 with atomically dispersed Pd as highly active catalyst for solvent-free aerobic oxidation of benzyl alcohol, Chem. Eng. J. 313 (2017) 1–9. doi:10.1016/j.cej.2016.12.024.
[13] M. Santonastaso, S.J. Freakley, P.J. Miedziak, G.L. Brett, J.K. Edwards, G.J. Hutchings, Oxidation of Benzyl Alcohol using in Situ Generated Hydrogen Peroxide, Org. Process Res. Dev. 18 (2014) 1455–1460. doi:10.1021/op500195e.
[14] M. Haruta, Catalysis of Gold Nanoparticles Deposited on Metal Oxides, CATTECH. 6 (2011) 102–115.
[15] M. Haruta, When Gold Is Not Noble: Catalysis by Nanoparticles, Chem. Rec. 3 (2003) 75–87. doi:10.1002/tcr.10053.
[16] H. Huang, X. Yang, Synthesis of polysaccharide-stabilized gold and silver nanoparticles: a green method, Carbohydr. Res. 339 (2004) 2627–2631. doi:10.1016/j.carres.2004.08.005.

[17] J. Belloni, M. Mostafavi, H. Remita, J.-L. Marignier, M.-O. Delcourt, Radiation-induced synthesis of mono- and multi-metallic clusters and nanocolloids, New J. Chem. 22 (1998) 1239–1255. doi:10.1039/a801445k.
[18] K. Okitsu, Y. Mizukoshi, T.A. Yamamoto, Y. Maeda, Y. Nagata, Sonochemical synthesis of gold nanoparticles on chitosan, Mater. Lett. 61 (2007) 3429–3431. doi:10.1016/j.matlet.2006.11.090.
[19] G.S. Métraux, C.A. Mirkin, Rapid Thermal Synthesis of Silver Nanoprisms with Chemically Tailorable Thickness, Adv. Mater. 17 (2005) 412–415. doi:10.1002/adma.200401086.
[20] A. Ghosh, C. Ranjan Patra, P. Mukherjee, M. Sastry, R. Kumar, Preparation and stabilization of gold nanoparticles formed by in situ reduction of aqueous chloroaurate ions within surface-modified mesoporous silica, Microporous Mesoporous Mater. 58 (2003) 201–211. doi:10.1016/S1387-1811(02)00626-1.
[21] J. Turkevich, P.C. Stevenson, J. Hillier, A study of the nucleation and growth processes in the synthesis of colloidal gold, Discuss. Faraday Soc. 11 (1951) 55. doi:10.1039/df9511100055.
[22] M. Brust, M. Walker, D. Bethell, D.J. Schiffrin, R. Whyman, Synthesis of thiol-derivatised gold nanoparticles in a two-phase Liquid–Liquid system, J Chem Soc Chem Commun. 0 (1994) 801–802. doi:10.1039/C39940000801.
[23] B.D. Busbee, S.O. Obare, C.J. Murphy, An Improved Synthesis of High-Aspect-Ratio Gold Nanorods, Adv. Mater. 15 (2003) 414–416. doi:10.1002/adma.200390095.
[24] C. Yang, P. Liu, Y. Ho, C. Chiu, K. Chao, Highly Dispersed Metal Nanoparticles in Functionalized SBA-15, Chem. Mater. 15 (2003) 275–280. doi:10.1021/cm020822q.
[25] Y.-J. Han, J.M. Kim, G.D. Stucky, Preparation of Noble Metal Nanowires Using Hexagonal Mesoporous Silica SBA-15, Chem. Mater. 12 (2000) 2068–2069. doi:10.1021/cm0010553.
[26] T. de Mattos Amadio, D. Hotza, J. Batista Rodrigues Neto, M. Blosi, A.L. Costa, M. Dondi, Bentonites functionalized by impregnation with TiO_2, Ag, Pd and Au nanoparticles, Appl. Clay Sci. 146 (2017) 1–6. doi:10.1016/j.clay.2017.05.028.
[27] A.M. Eremenko, N.P. Smirnoval, I.P. Mukhal, H.R. Yashan, Silver and gold nanoparticles in silica matrices: synthesis, properties, and application, Theor. Exp. Chem. 46 (2010) 65–88. doi:10.1007/s11237-010-9122-5.
[28] H.A. Schwarz, Free radicals generated by radiolysis of aqueous solutions, J. Chem. Educ. 58 (1981) 101. doi:10.1021/ed058p101.
[29] J.A. LaVerne, S.M. Pimblott, Diffusion-kinetic modeling of the electron radiolysis of water at elevated temperatures, J. Phys. Chem. 97 (1993) 3291–3297. doi:10.1021/j100115a034.
[30] W. Abidi, H. Remita, Gold based Nanoparticles Generated by Radiolytic and Photolytic Methods, Recent Pat. Eng. 4 (2010) 170–188. doi:10.2174/187221210794578556.
[31] G. Krylova, A. Eremenko, N. Smirnova, S. Eustis, Structure and spectra of photochemically obtained nanosized silver particles in presence of modified porous silica, Int. J. Photoenergy. 7 (2005) 193–198. doi:10.1155/S1110662X05000292.
[32] S. Eustis, G. Krylova, N. Smirnova, A. Eremenko, C. Tabor, W. Huang, M.A. El-Sayed, Using silica films and powders modified with benzophenone to photoreduce silver nanoparticles, J. Photochem. Photobiol. Chem. 181 (2006) 385–393. doi:10.1016/j.jphotochem.2005.12.024.
[33] L. Balan, V. Melinte, T. Buruiana, R. Schneider, L. Vidal, Controlling the morphology of gold nanoparticles synthesized photochemically in a polymer matrix through photonic parameters, Nanotechnology. 23 (2012) 415705. doi:10.1088/0957-4484/23/41/415705.

[34] T. Buruiana, V. Melinte, F. Jitaru, E.C. Buruiana, L. Balan, Preparation of siloxane-based urethane dimethacrylates carrying carboxylic groups and the effect of silver nanoparticles on the properties of composite polymer films, J. Polym. Sci. Part Polym. Chem. 50 (2012) 874–883. doi:10.1002/pola.25839.
[35] Y. Wan, Zhao, On the Controllable Soft-Templating Approach to Mesoporous Silicates, Chem. Rev. 107 (2007) 2821–2860. doi:10.1021/cr068020s.
[36] M.T. Bore, H.N. Pham, E.E. Switzer, T.L. Ward, A. Fukuoka, A.K. Datye, The Role of Pore Size and Structure on the Thermal Stability of Gold Nanoparticles within Mesoporous Silica, J. Phys. Chem. B. 109 (2005) 2873–2880. doi:10.1021/jp045917p.
[37] F. Wang, C. Liu, G. Liu, J. Liu, Amine functionalized mesoporous silica nanospheres supported gold nanoparticles: an effective catalyst for styrene epoxidation, J. Porous Mater. 22 (2015) 1423–1430. doi:10.1007/s10934-015-0022-x.
[38] D. Zhao, Triblock Copolymer Syntheses of Mesoporous Silica with Periodic 50 to 300 Angstrom Pores, Science. 279 (1998) 548–552. doi:10.1126/science.279.5350.548.
[39] Y. Peng, W. Leng, B. Dong, R. Ge, H. Duan, Y. Gao, Bottom-up preparation of gold nanoparticle-mesoporous silica composite nanotubes as a catalyst for the reduction of 4-nitrophenol, Chin. J. Catal. 36 (2015) 1117–1123. doi:10.1016/S1872-2067(14)60310-7.
[40] Y. Guari, C. Thieuleux, A. Mehdi, C. Reyé, R.J.P. Corriu, S. Gomez-Gallardo, K. Philippot, B. Chaudret, R. Dutartre, In situ formation of gold nanoparticles within functionalised ordered mesoporous silica via an organometallic 'chimie douce' approach, Chem. Commun. 0 (2001) 1374–1375. doi:10.1039/b102575a.
[41] Z. Kónya, V.F. Puntes, I. Kiricsi, J. Zhu, J.W. Ager, M.K. Ko, H. Frei, P. Alivisatos, G.A. Somorjai, Synthetic Insertion of Gold Nanoparticles into Mesoporous Silica, Chem. Mater. 15 (2003) 1242–1248. doi:10.1021/cm020824a.
[42] C. Aprile, A. Abad, H. García, A. Corma, Synthesis and catalytic activity of periodic mesoporous materials incorporating gold nanoparticles, J. Mater. Chem. 15 (2005) 4408. doi:10.1039/b507418e.
[43] B. Lee, H. Zhu, Z. Zhang, S.H. Overbury, S. Dai, Preparation of bicontinuous mesoporous silica and organosilica materials containing gold nanoparticles by co-synthesis method, Microporous Mesoporous Mater. 70 (2004) 71–80. doi:10.1016/j.micromeso.2004.03.004.
[44] P. Mukherjee, M. Sastry, R. Kumar, Size discrimination of colloidal nanoparticles by thiol-functionalized MCM-41 mesoporous molecular sieves, PhysChemComm. 3 (2000) 15. doi:10.1039/b002419h.
[45] M. Haruta, Nanoparticulate Gold Catalysts for Low-Temperature CO Oxidation, ChemInform. 35 (2004). doi:10.1002/chin.200448226.
[46] M. Okumura, S. Nakamura, S. Tsubota, T. Nakamura, M. Azuma, M. Haruta, Chemical vapor deposition of gold on Al_2O_3, SiO_2, and TiO_2 for the oxidation of CO and of H_2, Catal. Lett. 51 (1998) 53–58.
[47] M. Daté, M. Okumura, S. Tsubota, M. Haruta, Vital Role of Moisture in the Catalytic Activity of Supported Gold Nanoparticles, Angew. Chem. Int. Ed. 43 (2004) 2129–2132. doi:10.1002/anie.200453796.
[48] Z. Gui, W. Cao, L. Chen, Z. Qi, Propene carbonate intensified cyclohexane oxidation over Au/SiO_2 catalyst, Catal. Commun. 64 (2015) 58–61. doi:10.1016/j.catcom.2015.02.001.
[49] D. Gao, X. Zhang, X. Dai, Y. Qin, A. Duan, Y. Yu, H. Zhuo, H. Zhao, P. Zhang, Y. Jiang, J. Li, Z. Zhao, Morphology-selective synthesis of active and durable gold catalysts with high

catalytic performance in the reduction of 4-nitrophenol, Nano Res. 9 (2016) 3099–3115. doi:10.1007/s12274-016-1193-8.
[50] N. Fattori, C.M. Maroneze, L.P.D. Costa, M. Strauss, I.O. Mazali, Y. Gushikem, Chemical and photochemical formation of gold nanoparticles supported on viologen-functionalized SBA-15, Colloids Surf. Physicochem. Eng. Asp. 437 (2013) 120–126. doi:10.1016/j.colsurfa.2012.11.022.
[51] C.M. Maroneze, L.P. da Costa, F.A. Sigoli, Y. Gushikem, I.O. Mazali, One-step preparation of silver nanoparticles confined in functionalized-free SBA-15 channels, Synth. Met. 160 (2010) 2099–2103. doi:10.1016/j.synthmet.2010.07.037.
[52] A. Fukuoka, H. Araki, Y. Sakamoto, S. Inagaki, Y. Fukushima, M. Ichikawa, Palladium nanowires and nanoparticles in mesoporous silica templates, Inorganica Chim. Acta. 350 (2003) 371–378. doi:10.1016/S0020-1693(02)01541-4.
[53] W. Chen, J.-Y. Zhang, Y. Di, I.W. Boyd, Photo-chemical production of gold nanoparticles in monolithic porous silica by using a novel excimer ultraviolet source, Inorg. Chem. Commun. 6 (2003) 950–952. doi:10.1016/S1387-7003(03)00158-8.
[54] Y. Belmoujahid, M. Bonne, Y. Scudeller, D. Schleich, Y. Grohens, B. Lebeau, SBA-15 mesoporous silica as a super insulating material, Eur. Phys. J. Spec. Top. 224 (2015) 1775–1785. doi:10.1140/epjst/e2015-02498-3.
[55] A. Usher, D.C. McPhail, J. Brugger, A spectrophotometric study of aqueous Au(III) halide–hydroxide complexes at 25–80°C, Geochim. Cosmochim. Acta. 73 (2009) 3359–3380. doi:10.1016/j.gca.2009.01.036.
[56] M. Harada, S. Kizaki, Formation Mechanism of Gold Nanoparticles Synthesized by Photoreduction in Aqueous Ethanol Solutions of Polymers Using In Situ Quick Scanning X-ray Absorption Fine Structure and Small-Angle X-ray Scattering, Cryst. Growth Des. 16 (2016) 1200–1212. doi:10.1021/acs.cgd.5b01168.
[57] A. Zuber, M. Purdey, E. Schartner, C. Forbes, B. van der Hoek, D. Giles, A. Abell, T. Monro, H. Ebendorff-Heidepriem, Detection of gold nanoparticles with different sizes using absorption and fluorescence based method, Sens. Actuators B Chem. 227 (2016) 117–127. doi:10.1016/j.snb.2015.12.044.
[58] J. Rodríguez-Fernández, J. Pérez-Juste, P. Mulvaney, L.M. Liz-Marzán, Spatially-Directed Oxidation of Gold Nanoparticles by Au(III)−CTAB Complexes, J. Phys. Chem. B. 109 (2005) 14257–14261. doi:10.1021/jp052516g.
[59] S. Underwood, P. Mulvaney, Effect of the Solution Refractive Index on the Color of Gold Colloids, Langmuir. 10 (1994) 3427–3430. doi:10.1021/la00022a011.
[60] W. Haiss, N.T.K. Thanh, J. Aveyard, D.G. Fernig, Determination of Size and Concentration of Gold Nanoparticles from UV−Vis Spectra, Anal. Chem. 79 (2007) 4215–4221. doi:10.1021/ac0702084.
[61] V. Amendola, M. Meneghetti, Size Evaluation of Gold Nanoparticles by UV−vis Spectroscopy, J. Phys. Chem. C. 113 (2009) 4277–4285. doi:10.1021/jp8082425.
[62] J. Luo, O. Ersen, W. Chu, T. Dintzer, P. Petit, C. Petit, Anchoring and promotion effects of metal oxides on silica supported catalytic gold nanoparticles, J. Colloid Interface Sci. 482 (2016) 135–141. doi:10.1016/j.jcis.2016.08.001.
[63] J.-P. Jasmin, F. Miserque, E. Dumas, I. Vickridge, J.-J. Ganem, C. Cannizzo, A. Chaussé, XPS and NRA investigations during the fabrication of gold nanostructured functionalized screen-printed sensors for the detection of metallic pollutants, Appl. Surf. Sci. 397 (2017) 159–166. doi:10.1016/j.apsusc.2016.11.125.

[64] Z. Qu, G. Ke, Y. Wang, M. Liu, T. Jiang, J. Gao, Investigation of factors influencing the catalytic performance of CO oxidation over Au–Ag/SBA-15 catalyst, Appl. Surf. Sci. 277 (2013) 293–301. doi:10.1016/j.apsusc.2013.04.051.
[65] Y. Zhang, J. Deng, L. Zhang, W. Qiu, H. Dai, H. He, AuOx/$Ce_{0.6}Zr_{0.3}Y_{0.1}O_2$ nano-sized catalysts active for the oxidation of methane, Catal. Today. 139 (2008) 29–36. doi:10.1016/j.cattod.2008.08.005.
[66] M. Zaier, L. Vidal, S. Hajjar-Garreau, J.-L. Bubendorff, L. Balan, Tuning the morphology of silver nanostructures photochemically coated on glass substrates: an effective approach to large-scale functional surfaces, Nanotechnology. 28 (2017) 105603. doi:10.1088/1361-6528/28/10/105603.
[67] F.-Z. Su, M. Chen, L.-C. Wang, X.-S. Huang, Y.-M. Liu, Y. Cao, H.-Y. He, K.-N. Fan, Aerobic oxidation of alcohols catalyzed by gold nanoparticles supported on gallia polymorphs, Catal. Commun. 9 (2008) 1027–1032. doi:10.1016/j.catcom.2007.10.010.
[68] C.P. Ferraz, M.A.S. Garcia, É. Teixeira-Neto, L.M. Rossi, Oxidation of benzyl alcohol catalyzed by gold nanoparticles under alkaline conditions: weak vs. strong bases, RSC Adv. 6 (2016) 25279–25285. doi:10.1039/C6RA01795A.
[69] S. Biella, L. Prati, M. Rossi, Selective Oxidation of D-Glucose on Gold Catalyst, J. Catal. 206 (2002) 242–247. doi:10.1006/jcat.2001.3497.
[70] T. Pasini, M. Piccinini, M. Blosi, R. Bonelli, S. Albonetti, N. Dimitratos, J.A. Lopez-Sanchez, M. Sankar, Q. He, C.J. Kiely, G.J. Hutchings, F. Cavani, Selective oxidation of 5-hydroxymethyl-2-furfural using supported gold–copper nanoparticles, Green Chem. 13 (2011) 2091. doi:10.1039/c1gc15355b.
[71] B.N. Zope, D.D. Hibbitts, M. Neurock, R.J. Davis, Reactivity of the Gold/Water Interface During Selective Oxidation Catalysis, Science. 330 (2010) 74–78. doi:10.1126/science.1195055.
[72] S. Ivanova, V. Pitchon, C. Petit, Application of the direct exchange method in the preparation of gold catalysts supported on different oxide materials, J. Mol. Catal. Chem. 256 (2006) 278–283. doi:10.1016/j.molcata.2006.05.006.
[73] C. Megías-Sayago, L.F. Bobadilla, S. Ivanova, A. Penkova, M.A. Centeno, J.A. Odriozola, Gold catalyst recycling study in base-free glucose oxidation reaction, Catal. Today. 301 (2018) 72–77. doi:10.1016/j.cattod.2017.03.022.
[74] Y. Wang, S. Van de Vyver, K.K. Sharma, Y. Román-Leshkov, Insights into the stability of gold nanoparticles supported on metal oxides for the base-free oxidation of glucose to gluconic acid, Green Chem. 16 (2014) 719–726. doi:10.1039/C3GC41362D.
[75] B.N. Zope, R.J. Davis, Inhibition of gold and platinum catalysts by reactive intermediates produced in the selective oxidation of alcohols in liquid water, Green Chem. 13 (2011) 3484. doi:10.1039/c1gc15953d.